Article

Characteristics of Electrical Resistance Alteration during In-Situ Leaching of Ion-Adsorption Type Rare Earth Ore

Xiujuan Feng * and Xiaoqing Wang *

Posted Date: 12 December 2023

doi: 10.20944/preprints202312.0862.v1

Keywords: ion-adsorption type rare earth; in-situ leaching; electrochemical impedance spectroscopy; electrical resistance; equivalent circuit model

Article

Characteristics of Electrical Resistance Alteration during In-Situ Leaching of Ion-Adsorption Type Rare Earth Ore

Xiujuan Feng * and Xiaoqing Wang *

School of Mines, China University of Mining and Technology, Xuzhou, Jiangsu 221116, China
* xiujuanf@126.com or xjfeng@cumt.edu.cn (X.F.); xqwang2022@cumt.edu.cn (X.W.)

Abstract: The chemical reaction of ion-adsorption type rare earth during in-situ leaching process is accompanied by ion migration and charge movement, making the leaching process electrochemical in nature. The chemical reaction rate plays an important role in the leaching rate of rare earth elements. In this work, electrochemical impedance spectroscopy (EIS) was used to reveal characteristics of electrical resistance alteration and leaching rate of rare earth elements during in-situ leaching. The equivalent circuit model of the leaching process was established, and two critical parameters of solution resistance Rs and charge transfer resistance Rt were analyzed to reflect the electrochemical characteristics. According to the characteristics of electrical resistance alteration, the leaching process was divided into four stages: wetting, reaction, equilibrium, and top water stage. The resistance parameters Rs and Rt decreased first and then increased during the leaching process. The maximum value of Rs was 1330Ω·cm^2 at the end of the top water stage, and the minimum value was 135Ω·cm^2 at the beginning of the equilibrium stage. The maximum value of Rt was 8310Ω·cm^2 at the beginning of the leaching stage, and the minimum value was 21Ω·cm^2 at the end of the reaction stage. Rs and Rt were negatively correlated with the pore size and chemical reaction rate during leaching. With increasing of pore size and reaction rate , the resistance parameter decrease. This study provide a new idea for intelligent monitoring of rare earth ore.

Keywords: ion-adsorption type rare earth; in-situ leaching; electrochemical impedance spectroscopy; electrical resistance; equivalent circuit model

1. Introduction

Rare earth elements (REEs), especially for the mid and heavy REEs, are essential in high-tech industries such as renewable energy, national defense and new materials preparation [1–3]. Owing to their special 4f electron layer structure, they can exhibit some unique optical, magnetic, and electrical properties [4,5]. Ion-adsorption rare earth ores are rich in medium and heavy rare earth elements [6–9] and are strategic mineral resources [10,11]. The rare earth content of ionic rare earth ores is generally 0.05–0.2 wt.% REO [12]. It usually presents in four phases: water soluble phase, ion-exchanged phase, mineral phase and colloidal sediment phase [13–15]. The ion-exchanged phase accounts for 60-90% of the whole-phase rare earth [16,17] and the ion-exchangeable phase rare earth is adsorbed on the surface of clay minerals such as kaolin and mica in the form of hydrated cations or hydroxyl hydrated ions [18–20].

The surface of the clay mineral is negatively charged and has a fixed surface electrostatic potential, which attracts counterions into the electrolyte solution to form a double layer [21,22]. The ion-adsorption type rare earth ore is mainly composed of the clay minerals, which will attract rare earth ions in the natural environment, forming double elecrotic layer. The leaching process of ion-adsorbed rare earth is essentially a process of cation adsorption by the lixiviant, desorption of rare earth ions, and redevelopment of the double elecrotic layer on the clay surface [23]. The thickness of double layer is related to the valence number of ions in the leach solution, ion concentration, temperature, and pH [19,24]. An inorganic salt solution is used as the lixiviant, and rare earth

 doi:10.20944/preprints202312.0862.v1

elements are leached through ion-exchange [25–27]. Ammonium sulfate is a widely used lixiviant for ion adsorption rare earth due to its advantages of high exchangeability of ammonium ions and low cost [18,28,29]. Ammonium ions in the lixiviant are exchanged with rare earth ions, and rare earth ions enter the leaching solution [30,31]. The equation for the ion-exchange reaction that occurs during leaching is as follows (where s represents the solid phase; aq represents the liquid phase):

$$[Al_4Si_4O_{10}(OH)_8]_m \cdot nRE^{3+}(s)+3nNH_4^+(aq) \rightleftharpoons [Al_4Si_4O_{10}(OH)_8]_m \cdot [NH_4^+]_{3n}(s)+nRE^{3+}(aq) \quad (1)$$

Clay mineral particles have an unbalanced charge on their surfaces and have a range of electrochemical properties [32], such as conductive properties of electrolyte and ion transport properties. The migration of ions and chemical reactions at the liquid-solid interface also trigger electrical phenomena during in-situ leaching. Electrochemical impedance spectroscopy has been widely applied by scholars to investigate the mechanical properties of contaminated soil remediation, the corrosion behavior of cement materials, the mechanical properties of concrete materials, the microscopic pore structure of solid waste materials, and the hydration process of cement [33–37]. This method can reflect the chemical reactions and microstructural changes occurring within the substance under test and reveal the interfacial reactions between the conducting phases. Soil is a three-phase medium of solids, liquids, and gases that can be structured as an electrochemical system. Ion-adsorption rare earth are clay minerals and the EIS technique is equally applicable. Physical and chemical interactions between the leaching solution and the mineral particles occur during the leaching process of rare earth ore, which can be continuously monitored using EIS technology.

In this study, electrochemical impedance test of the ammonium sulfate leaching process was carried out by combining the previous studies on the EIS theory and its application by Macdonald J R [38], Meilun Shi [39] and Chunan Cao [40], as well as by referring to the studies on the electrochemical impedance change of clay and its influencing factors by Zhao [41], A. Elmelouky [42] and others. Combined with Nyquist and Bode diagrams and equivalent circuit element parameters, the electrochemical characterization of the whole leaching process was monitored. An equivalent circuit model applicable to the leaching process was established to explore the resistance change of the leaching process of rare earth ores, to reveal the charge migration law in the pore solution and at the solid-liquid interface, and to analyze the changing law of the pore structure and the chemical reaction in the leaching process. The electrical resistance variation characteristics of ion-adsorbed rare earth ore during in-leaching process can reflect the rare earth leaching process and leaching efficiency, which can provide more ideas for the intelligent mining of rare earth ores, the optimization of leaching process and the improvement of leaching efficiency.

2. Materials and Methods

2.1. Test Materials

The raw materials were from an ionic rare earth mine in Dingnan County, Ganzhou City, Jiangxi Province, China. The water content of the rare earth ore was determined to be 11.2%. The particle size distribution of the raw ore is shown in Table 1.

Table 1. Particle size distribution of raw ore (w/%).

particle size /mm	<0.1	0.1~0.5	0.5~0.9	0.9~1.43	1.43~4	>4
percentage /%	14.6	16.2	13.2	15.7	19.2	21.1

Inductively Coupled Plasma Optical Emission Spectrometer (ICP-OES) was used to detect the rare earth content of different particle sizes, and the results are shown in Table 2.

Table 2. Distribution of rare earth content in different grain sizes.

Particle Size /mm	−0.15	0.15–0.25	0.25–0.45	0.45–0.9	0.9–1.43	1.43–4	+4
Rare Earth Content Distribution /%	53.82	15.63	11.16	10.76	3.70	2.83	2.11

 doi:10.20944/preprints202312.0862.v1

As shown in Tables 1 and 2, the proportion of mineral particles with a particle size of less than 1.43mm is greater than 50%, indicating that the original ore has a finer particle size and a higher degree of weathering. Mineral particles below 0.15mm in size have the highest rare earth content, accounting for 53.82% of the total rare earth and smaller size mineral particles contain higher rare earth content.

2.2. Test Methods

2.2.1. Column Immersion Test

Ionic rare earth in-situ leaching simulation tests were conducted using ammonium sulfate solution as lixiviant. Some rare earth ore samples were weighed and dried at 100°C for 12h. 200 g of dried rare earth ore samples were weighed, mixed thoroughly, and added to a leaching column of Φ59 mm*90 mm. A filter paper was placed above the samples, and a test electrode was fixed into the rare earth ore samples. A funnel and a collecting cylinder were placed below the column, with filter paper inside the funnel. Ammonium sulfate was used as the lixiviant, with a concentration of 0.1 mg/mL, a flow rate of 1.5 mL/min, a solid-liquid ratio of 1:2, pH=4, and ambient temperature.

2.2.2. Electrochemical Impedance Spectroscopy Tests

Electrochemical impedance spectroscopy is a method of electrochemical measurements in which a sinusoidal potential (or current) of a certain amplitude is used as a perturbation signal, resulting in an approximately linear relationship between the perturbation and the system's response. EIS testing was performed throughout the column leach test using the admiral squidstat series of electrochemical equipment. The leach solution was collected at regular intervals. The parameters of the rare earth leaching process were set as follows: AC sinusoidal signal amplitude of 10 mV, test frequency of 10^{-2}–10^{6} Hz, and three-electrode method, with the working electrode being a graphite electrode, the auxiliary electrode being a platinum electrode, and the reference electrode being an Ag/AgCl electrode. The Nyquist and Bode plots obtained from the test were fitted and analyzed using Zahner Analysis software to obtain the electrochemical component parameters of the ionic rare earth during the in-situ leaching process. Figure 1 shows the test equipment of this study.

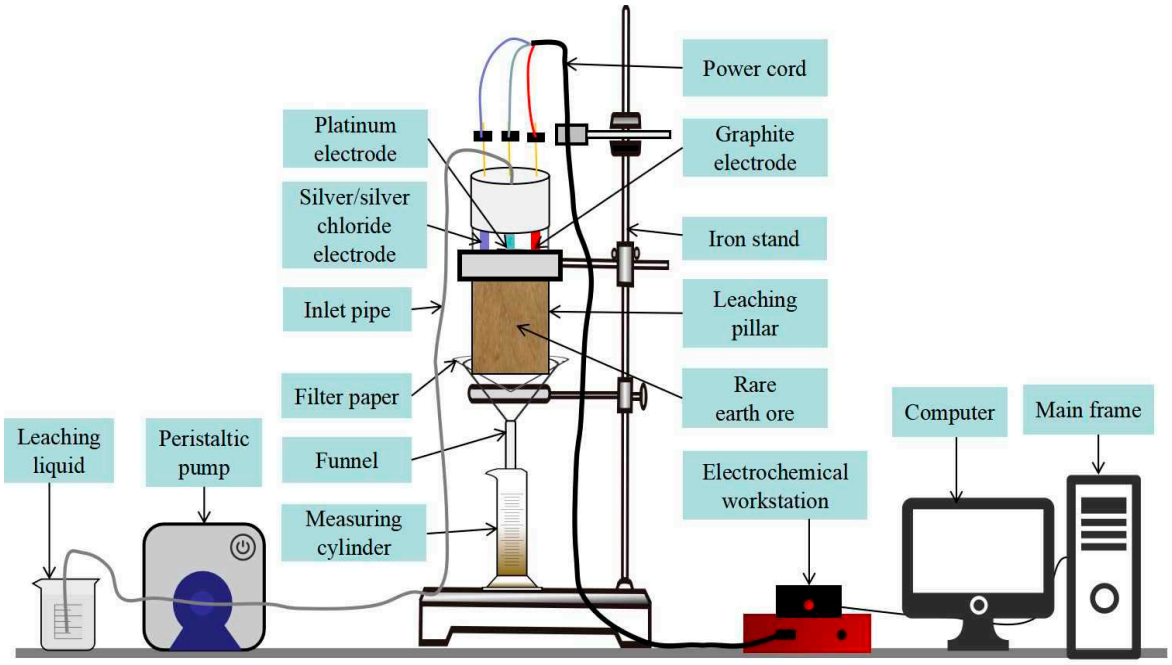

Figure 1. Diagram of column immersion and EIS test equipment.

Preprints (www.preprints.org) | NOT PEER-REVIEWED | Posted: 12 December 2023 doi:10.20944/preprints202312.0862.v1

3. Equivalent circuit model

3.1. Analysis of Conductive Pathways

The ionic rare earth in-situ leaching process includes three media: solid, liquid, and gas. The internal conductive path of the ore body mainly includes the conduction of the rare earth particles, the conduction between the particles pore liquid and the conduction between the rare earth particles and the solid-liquid interface of the pore liquid [43,44]. The conductive path is shown in Figure 2.

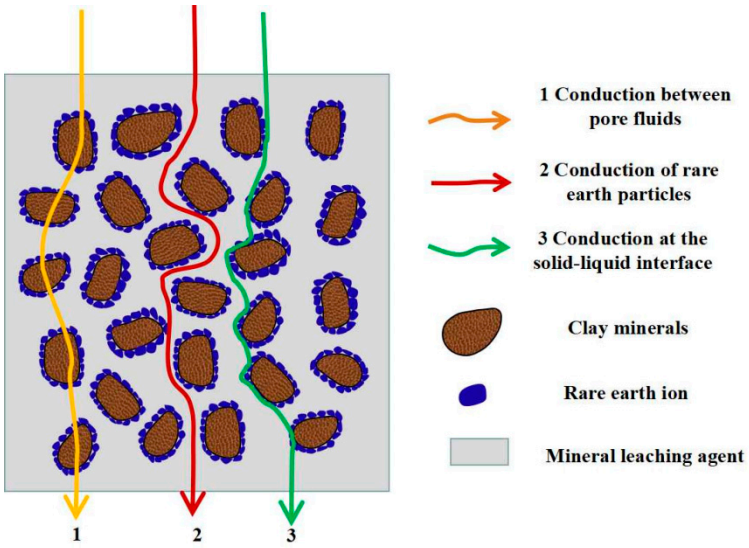

Figure 2. Conductive paths during in-situ leaching of ionic rare earth.

Among the three conductive paths, the first conduction is rare earth particles. Since they contain a certain amount of water and exist in the natural electrolyte solution for a long time, they are electrically conductive. However, the conductivity of the rare earth particles is minimal and can be ignored due to the limited water content and electrolyte solution concentration. The second type is the pore liquid conductivity in the in-situ leaching process, which is mainly induced by the ion-exchange reaction. The displacement reaction between pore liquid cations and rare earth cations leads to the migration of ions in pore liquid. The third type of solid-liquid interface conductivity is mainly caused by ion-exchange reactions. The second and third conductive effects are interrelated and interdependent , resulting from the ions in the pore liquid and the surface of rare earth particles have always existed in the physical and chemical reactions in the effective reaction stage of in-situ leaching. The ions in the pore liquid enter the solid-liquid interface through the ion-exchange reaction and eventually migrate to the surface of the rare earth particles.

3.2. Equivalent Circuit Model

An equivalent electrical circuit consists of continuously connected elements such as resistance, capacitance and inductance. The method is called the equivalent circuit method when the frequency response properties of the test material are the same as the electrical circuit described above. The equivalent circuit method can test the AC impedance spectrum because different electrochemical components have different frequency response times under the same current passage conditions. Resistive elements have the fastest response to current compared to other element and the capacitor can be considered a wire when the frequency is high. No electrochemical transfer occurs because it takes time for the ions to diffuse from the beginning of their movement. Therefore, the low-frequency region is controlled by the diffusion process.

In electrochemical reactions, there are two simultaneous processes: The first is a non-faraday process involving charging and discharging of the double layer capacitance when electrode potential is changed. The second is a faraday process involving charge transfer and diffusion at a certain

Preprints (www.preprints.org) | NOT PEER-REVIEWED | Posted: 12 December 2023 doi:10.20944/preprints202312.0862.v1

electrode potential, which is represented by the series connection of R_t and Z_w. These two processes are represented by a parallel circuit and there is a "dispersion effect" in the equivalent circuit fitting process. Due to the inhomogeneity of the electrode surface, the double layer capacitance is not a constant but a value that changes with frequency, and this phenomenon of capacitance change with frequency is called the dispersion effect. The dispersion effect reflects the instability of the parameters and the constant phase angle element CPE is used to represent the double layer capacitance to avoid this phenomenon. In the present study, based on the two processes of electrochemical reaction and leaching mechanism of ion-adsorption rare earth, the equivalent circuit of circuit elements was established as a quasi-Randles model based on the Randles model [45], as shown in Figure 3.

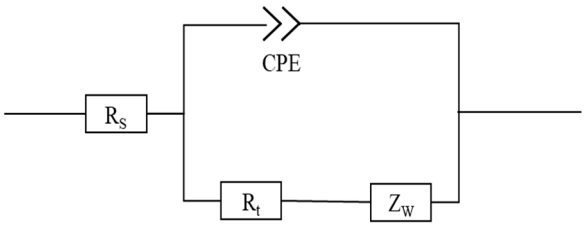

Figure 3. Quasi-Randles model equivalent circuit.

In Figure 3, Rs is the solution resistance, indicating the conductivity of the pore solution. Rt is the charge transfer resistance, reflecting the ease of charge transfer. Zw is the diffusion impedance, indicating the impedance of the reactants diffusing from the solution to the reaction surface of the electrode. CPE is the constant phase-angle element, which indicates the double elecrotic layer at the interface between the electrode and the solution, equivalent to a capacitor.

Figure 4 shows the Nyquist diagram of the equivalent circuit model. The high-frequency region shows a circular arc, which is controlled by the dynamics. The low-frequency region shows a slash at an angle of 45° to the real axis, which is controlled by material transfer (diffusion control). The curve intercept to the real axis in the high-frequency region is Rs, the diameter of the semicircle in the high-frequency region is Rt, and the intercept of the slanting line in the low-frequency region on the real axis is σ. The diameter of the impedance arc is deflected downward by an Angle φ relative to the real axis, which is called the dispersion angle. The CPE is represented by the two parameters, CPE-T and CPE-P, in which CPE-T denotes the charged amount of the double layer and the capacitance of its diffusion layer, and CPE-P is a parameter related to the diffusion angle ϕ, where ϕ is expressed as:

$$\phi = \pi(1-\text{CPE-P})/2 \quad (2)$$

Z_w is the diffusion impedance, which can be expressed by the diffusion coefficient:

$$Z_w = \sigma\omega_3^{-1/2}(1-j) \quad (3)$$

Where σ is the diffusion coefficient, $(\Omega\text{-cm}^2)/s^{1/2}$, ω_3 is the angular frequency, and j is an imaginary unit.

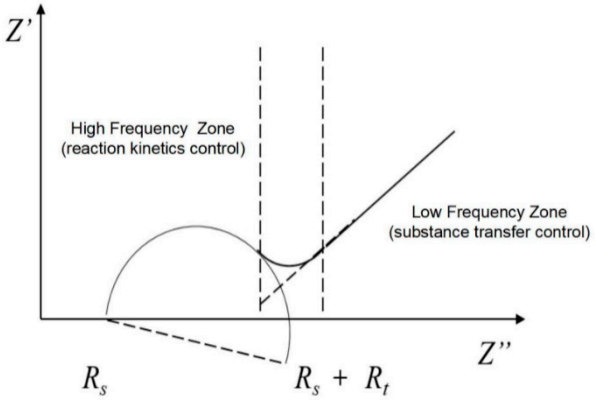

Preprints (www.preprints.org) | NOT PEER-REVIEWED | Posted: 12 December 2023 doi:10.20944/preprints202312.0862.v1

Figure 4. Nyquist plot for the quasi-Randles model.

4. Results and Analysis

4.1. Nyquist Plot Analysis

Figure 5 shows the three-dimensional diagram of the AC impedance spectrum of the whole leaching process of ion-adsorption rare earth using ammonium sulfate leaching. In order to facilitate the study and comparative analysis, the whole leaching process was divided into four stages including the wetting stage (30-50min), reaction stage (50-80min), equilibrium stage (80-250min), and top water stage (250-350min), according to the reaction time, reaction phenomenon, and impedance value change of the reaction process. Among them, the wetting stage refers to the process from the beginning of the ore body to the leaching fluid outflow. The reaction stage refers to the process from the beginning of the leaching solution to the significant change in impedance. The equilibrium stage refers to the process in which the impedance value is relatively stable. In the top water stage, the leaching solution was finished and deionized water was added to flush the ore body until the end.

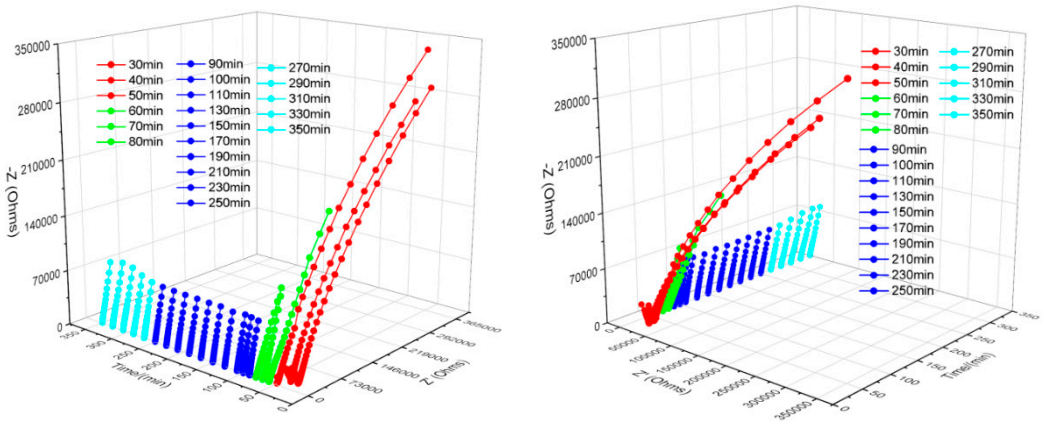

Figure 5. Three-dimensional diagram of the AC impedance spectrum of the leaching process.

As shown in Figure 6, the Nyquist curve was composed of the capacitance reactable arc in the high-frequency region (greater than 1000Hz) and the inclined straight line in the low-frequency region (less than 1Hz), which conformed to the quasi-Randles model. It was found that the capacitive reactance arc and the slope of the line changed significantly in the wetting stage, reaction stage and top water stage, while changed little in the equilibrium stage. The capacitive reactance arc radius and the capacitive reactance arc intercept to the real axis in the wetting and reaction stages decreased with the increase of reaction the increase of reaction time, indicating that the solution and charge transfer resistance in the two stages decreased. In the wetting and equilibrium stage, the slope of the straight line and the straight line intercept to the real axis decreased, indicating that the diffusion coefficient σ decreased. The diffusion coefficient was proportional to the resistance, and the resistance decreased continuously.

Preprints (www.preprints.org) | NOT PEER-REVIEWED | Posted: 12 December 2023 doi:10.20944/preprints202312.0862.v1

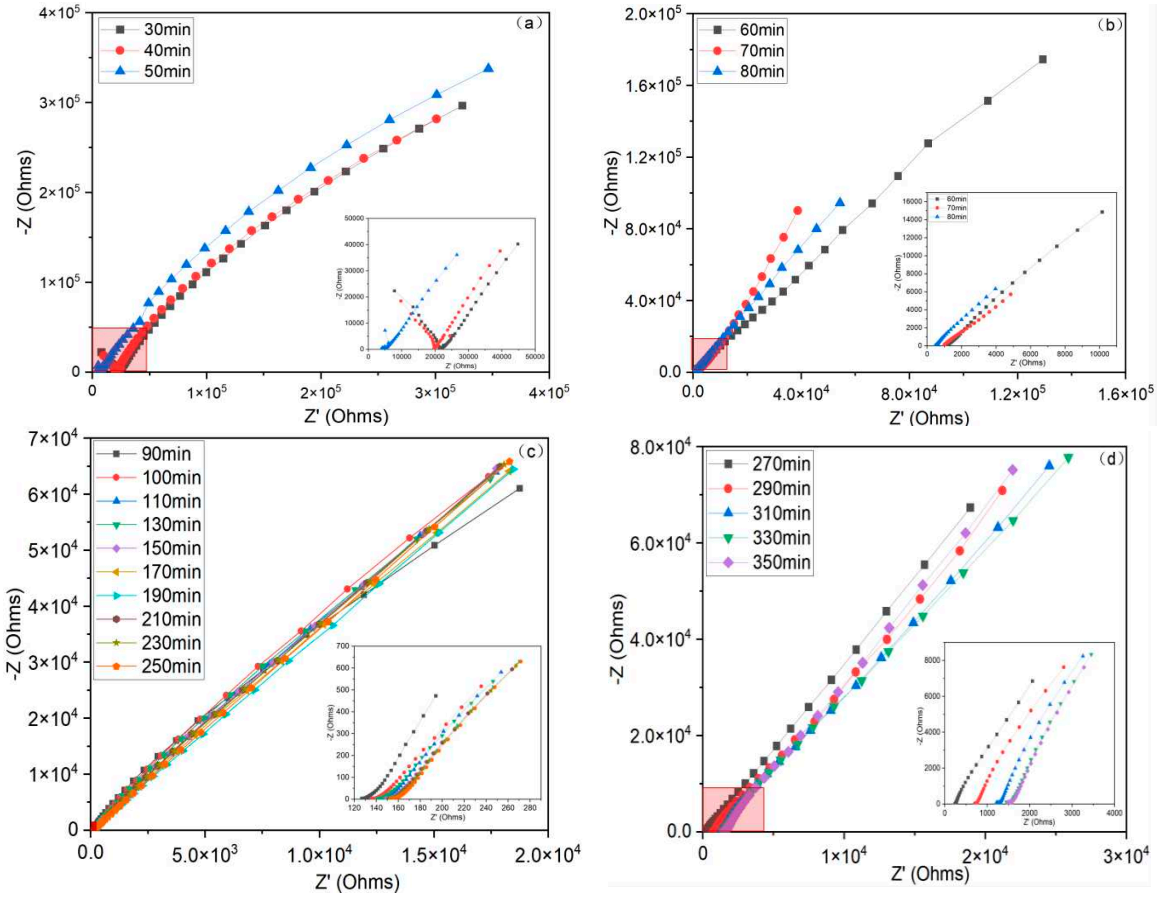

Figure 6. Nyquist diagram of ionic rare earth ore leaching process. (**a**)wetting stage (30–50 min);(**b**) reaction stage (50–80 min); (**c**) equilibrium stage (80–250 min); (**d**) top water stage (250–350min).

It can be inferred that in the wetting stage and the reaction stage, the ion concentration in the pore liquid kept increasing and the ion-exchange reaction at the solid-liquid interface kept increasing. The diffusion rate of ions in the pore liquid of the orebody was getting faster and faster and the ion concentration difference at the solid-liquid interface was getting larger and larger, which was conducive to the diffusion.

In the equilibrium stage, the impedance amplitude changed little, and the capacitive reactance arc radius was small. The capacitive reactance arc intercept to the real axis and the intercept of a line to the real axis has not changed significantly, indicating that the resistance value changed little. The ion-exchange reaction tended to be stable and the resistance at the top water stage increased significantly. The capacitive reactance arc radius and the capacitive reactance intercept to the real axis increased with time. The linear intercept to real axis increased, the diffusion coefficient σ increased and the resistance increased. The results indicated that the ion concentration decreased and the ion-exchange reaction intensity decreased significantly with the addition of deionized water.

4.2. Bode Plot Analysis

Figure 7 shows the frequency-impedance modulus plot for the leaching process of ion-adsorption rare earth.

Preprints (www.preprints.org) | NOT PEER-REVIEWED | Posted: 12 December 2023 doi:10.20944/preprints202312.0862.v1

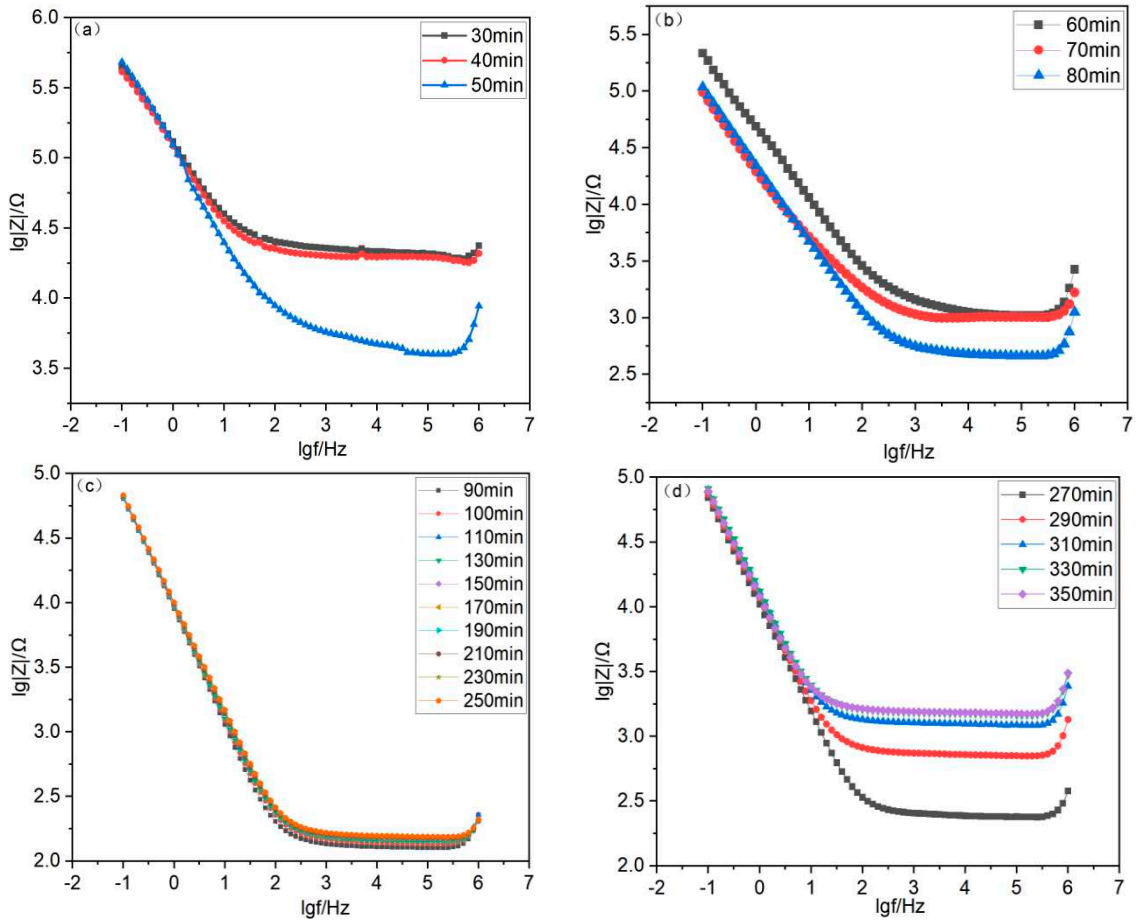

Figure 7. Diagram of impedance modulus of ionic rare earth ore leaching process. (**a**) wetting phase; (**b**) reaction phase; (**c**) equilibrium phase; (**d**) top water stage.

It can be seen from Figure 7 that the impedance modulus values in the four stages of the leaching process had a consistent decreasing with the frequency. In the frequency range of 10^{-1}-10^{2}, the curvature of the curve was large and the impedance modulus decreased linearly. In the frequency range of 10^{2}-10^{3} Hz, the curvature of the curve and the impedance modulus decreased slowly. In the frequency range of 10^{3}-10^{6} Hz, the change amplitude of the impedance modulus was small and tended to a certain value. During the leaching process, the impedance modulus decreased continuously in the wetting and reaction stages, then dropped to the lowest value and tended to be stable in the equilibrium stage. When deionized water was added, the impedance modulus gradually increased and tended to be stable in the final stage of top water.

As shown in Figure 8, the phase angle of the leaching process varies in the interval of 0-80°. In the wetting stage, the phase angle decreased with the frequency. The phase angle decreased rapidly when the frequency was 10-10^{3} Hz, and then decreased slowly when the frequency was less than 10 and more than 10^{3} Hz. In the reaction stage, the phase angle tended to increase first, then decrease and increase again. The phase angle increased rapidly and reached the peak when the frequency was less than 10 Hz, the phase angle decreased rapidly to nearly 0° when the frequency was 10-10^{3} Hz, and the phase angle increased again when the frequency was greater than 10 Hz. In the equilibrium stage, the phase angle peaked at 10^{-1}-10 Hz, decreased rapidly within 10-10^{3} Hz and remained basically stable within 10^{3}-10^{6} Hz. In the top water phase, the phase angle showed an overall decreasing trend, with a slight decrease within 0-10 Hz, followed by a rapid decrease within 10-10 kHz, and remained relatively stable within 10 k-1000 kHz. The wetting and equilibrium phases each had a peak, and the peak in each equivalent circuit corresponded to one time constant, indicating that time constants existed in both reaction phases [45].

Preprints (www.preprints.org) | NOT PEER-REVIEWED | Posted: 12 December 2023 doi:10.20944/preprints202312.0862.v1

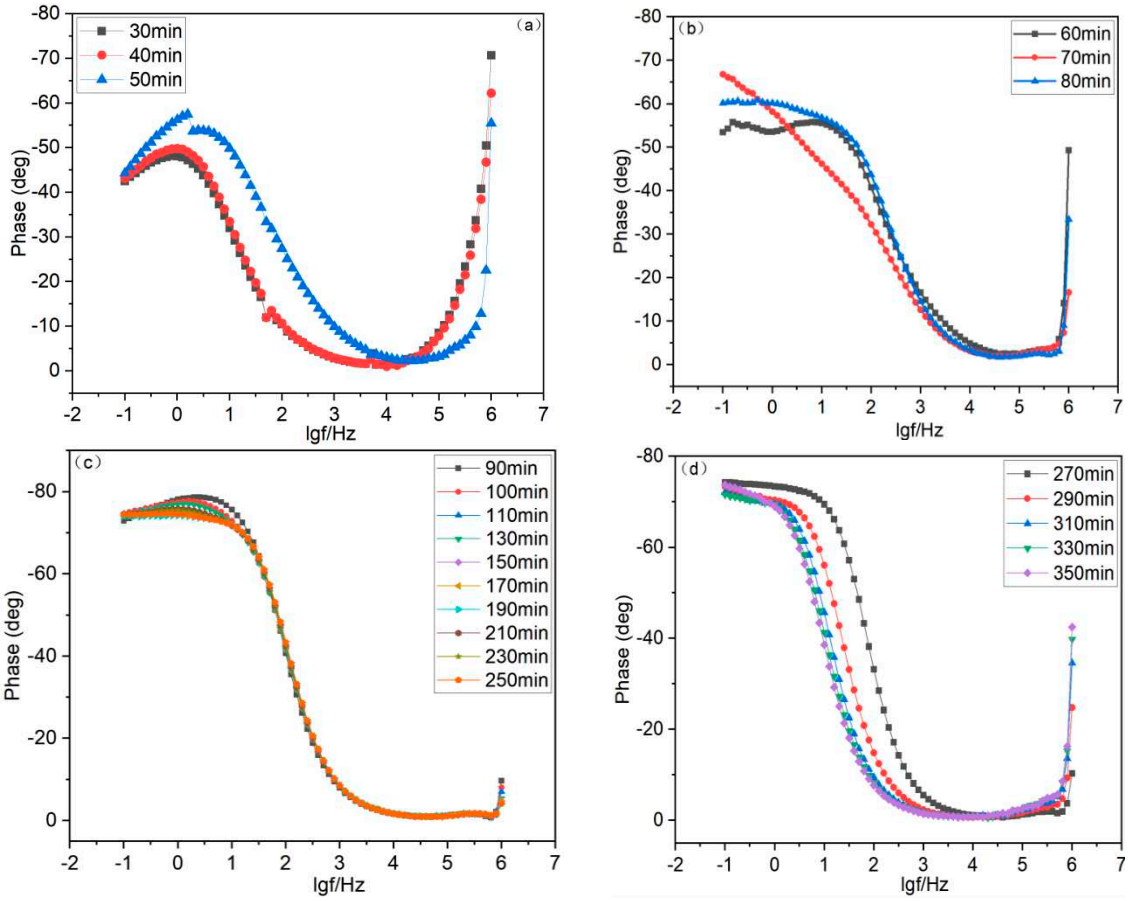

Figure 8. Phase angle change diagram of ionic rare earth ore during the leaching process. (a) wetting phase;(b) reaction phase;(c) equilibrium phase;(d) top water stage.

4.3. Equivalent Circuit Parameter Analysis

The Nyquist and Bode plots were fitted using Zahner Analysis software, and each equivalent circuit element parameter was fitted to obtain a fitting error of essentially less than 5%, as shown in Table 3.

Table 3. Equivalent circuit parameters of the leaching process.

Time(min)	R_s (Ω·cm²)	R_t (Ω·cm²)	Total error (%)
30	939	8310	3.77
40	538	571.9	2.31
50	453	528	4.89
60	334	310	2.25
70	235	256	2.45
80	140	21	2.62
90	135	23.9	3.85
100	136	22.7	2.5
110	145	47	1.76
130	140	25.6	2.1
150	149	43.1	1.52
170	151	45.5	1.87
190	153	32.6	2.01
210	151	30.9	1.62
230	152	43.8	1.71
250	154	47	1.95

Preprints (www.preprints.org) | NOT PEER-REVIEWED | Posted: 12 December 2023 doi:10.20944/preprints202312.0862.v1

270	246	25.7	2.55
290	697	51.6	2.58
310	1120	174	2.43
330	1240	223	2.07
350	1330	338	1.86

According to Table 3, the trend diagram of solution resistance and charge transfer resistance during leaching was drawn, as shown in Figure 9.

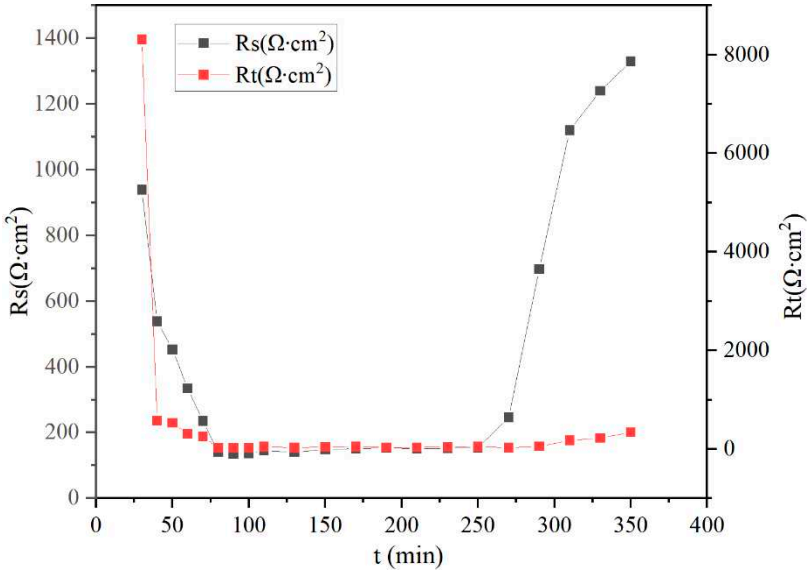

Figure 9. Trend diagram of solution resistance and charge transfer resistance during the leaching process.

Rs is the solution resistance, which mainly reflects the conductivity of the pore solution electrolyte of the orebody. The pore solution resistance is great and pore solution is difficult to conduct electricity when the Rs is large, which relates to the pore liquid and size [46,47]. From Table 3 and Figure 9, it can be seen that the solution resistance decreased at first and then increased during the leaching process. The solution resistance was 939Ω ·cm² at the wetting stage(30min), reached the minimum value of 135Ω ·cm² at the equilibrium stage(90min) and reached the maximum value of 1330Ω ·cm² at the top water stage(350min). It could be calculated that the ore sample was unsaturated with an unstable internal structure at the wetting stage. The pores inside the ore sample contained a large amount of gas, and micro and small holes dominated the pore structure. The pore connectivity between clay minerals was poor, and the pore solution had poor electrical conductivity, so the initial resistance value was considerable. From the beginning of the wetting stage to the 90th minute of the equilibrium stage, the addition of ammonium sulfate leach made the orebody transition from an "unsaturated state" to a "saturated state". The gas in the pores was gradually replaced by pore solution, and the pore solution volume, the saturation and the conductive path 2 in Figure 2 increased. The micro and small pores in the ore body evolve into medium and large pores under the action of seepage, and the pore size of the ore body increased, the seepage effect was enhanced, and the solution connectivity was improved [48–52]. Due to the continuous addition of ammonium sulfate leaching solution, the number of ions in the pore solution increased, and the improvement of pore connectivity led to the increase of the freely moving anions number in the solution, so the conductive capacity of the solution was enhanced.

From the 90th to the 250th minute of the equilibrium stage, the solution resistance fluctuated within 135-154 Ω·cm2 and showed a steady increase trend. The solution resistance in the equilibrium stage was significantly lower than that in the other three stages, indicating that an effective ion-

 doi:10.20944/preprints202312.0862.v1

exchange reaction was happening in the equilibrium stage. At the same time, the ore body had reached saturation [53] and the number of ions in the solution was relatively stable. Nevertheless, the pore structure of the ore body changed due to the ion-exchange reaction. The macropores number and the porosity decreased [54] and the solution connectivity deteriorated, which resulted in a slight increase in solution resistance with time in this stage. In the top water stage, the solution resistance showed a significant increasing trend due to the addition of deionized water inside the ore body. The ammonium sulfate solution and residual rare earth ions in the pore space were continuously discharged. The conductivity of deionized water was less than that of ammonium sulfate solution, so the resistance increased.

Rt is the charge transfer resistance, reflecting the ability of ions in the diffusion zone to complete charge transfer on the surface of ore body particles and the speed of electrochemical reaction [55], which is mainly determined by the ion concentration gradient and the adsorption characteristics of the ore body particles surface [24,26,27]. In the ion-exchange process, the ion-exchange reaction occurring on the surface of mineral particles desorbed rare earth ions to the binding liquid layer, resulting in a sharp increase in their concentration in the binding liquid layer. The adsorption of ammonium ions to mineral particles led to a rapid decrease in their concentration in the binding liquid layer, resulting in an apparent concentration gradient between the two layers, which promoted the directional migration of the two ions [56,57]. As shown in Table 3 and Figure 9, Rt generally presented a trend of first decreasing and then increasing, from the maximum value of 8,310ω ·cm2 in the wetting stage to the minimum value of 21Ω·cm2 at the 80th minute of the reaction stage. Rt reached 338Ω·cm2 at the end of the top water, and the resistance value in the equilibrium stage was close to the minimum value with a slight change.

According to the analysis above, it can be seen that at the beginning of the wetting stage, as the leaching solution entered the ore body, it took some time for the solution to penetrate into the ore body and diffused to the surface of the ore body particles to arise.

ion-exchange reaction. Therefore, the initial charge transfer was difficult, and the resistance value had an instantaneous maximum value. In the wetting and reaction stage, the number of ions in the ammonium sulfate solution increased and continuously entered the "diffusion double layer " region on the surface of the particles with the continuous penetration of the leaching solution, which led to the exchange of RE3+ and NH4+. In this process, the number of charges in the diffusion layer at the solid-liquid interface increased continuously, forming a significant concentration difference and promoting charge transfer. Meanwhile, according to the leaching reaction equation (1), nRE3+ (aq) resolved from the surface of the mineral particles and then continuously flowed out with the leaching solution, which promoted a positive reaction. The electrical resistance value showed a significant decrease [28] and reached a minimum value at the end of the reaction stage. From the 80th to the 100th minute, the resistance was minor and close to the minimum value, indicating that the ion-exchange reaction was dominant in this period. The ore body was interfered by external factors quickly, but the degree of interference was basically the same, so the resistance value changed little.

From the 100th minute of the equilibrium stage to the end of the equilibrium stage, the charge translation resistance increased in general and fluctuated up and down irregularly. During this period, the ion-exchange reaction continued, but the ion migration in the solution was hindered due to the decrease of porosity. Therefore, the number of ions in the diffusion layer at the solid-liquid interface decreased, the charge migration was inhibited and the resistance increased. As more and more rare earth ions were replaced, the amount of negative charge carried on the surface of mineral particles increased and the water film become thicker, which led to stronger retention effect on the fluid, weaker penetration effect and lower charge transfer ability. However, compared with the other three stages, the "effective leaching" mainly occurred in ion-exchange reaction, so the resistance was small. In the top water stage, the addition of deionized water led to a decrease in the concentration of ions in the solution, and the continuous occurrence of leaching reaction also reduced the content of rare earth ions in the ore body, resulting in a significant decrease in the number of ions in the diffused double electric layer. The charge transfer became difficult, and the resistance value increased continuously until the end of the top water.

5. Conclusions

This paper used electrochemical impedance spectroscopy (EIS) to study the electrochemical characterization of ionic rare earth during the in-situ leaching process, and an equivalent circuit model was established. Through the calculation of the fitted EIS parameters, the changing law of electrochemical parameters in the leaching process was obtained, and the parameters were analyzed and interpreted. The main conclusions were drawn as follows:

(1) Based on the electrochemical characterization of the in-situ leaching process of ion-adsorption rare earth, an equivalent circuit model was proposed to reflect the electrochemical changes of the leaching process. The main circuit elements of the model included a solution resistor, a charge transfer resistor, a constant phase angle element, and a diffusion impedance. The solution resistance Rs and charge transfer resistance Rt were mainly analyzed. The solution resistance reflected the number of ions in the ammonium sulfate solution and the change of pore structure of the ore body during leaching. The charge transfer resistance reflected the ion concentration gradient and chemical reaction at the liquid-solid interface during the leaching process, which were the main factors affecting the leaching and leaching rates.

(2) According to the changing law of electrochemical parameters of the leaching process, the leaching process was divided into four stages: wetting stage, reaction stage, equilibrium stage and top water stage. During the leaching process, the resistance parameters Rs and Rt values tended to decrease first and then increase. The maximum value of Rs was 1330Ω·cm2 at the end of the top water stage, and the minimum value was135Ω·cm2 at the beginning of the equilibrium stage. The maximum value of charge transfer resistance was 8,310 Ω·cm2 at the beginning of the leaching stage, and the minimum value was 21Ω·cm2 at the end of the reaction stage. Rs and Rt in the equilibrium leaching stage were close to the minimum value and remained relatively stable.

(3) The values of Rs and Rt were negatively correlated with the size of the pore structure and the chemical reaction rate of ion-exchange. The pore structure was large and the rate of chemical reaction was great when the resistance parameter value was small. At this stage, the pore solution connectivity of the ore body was good and the solid-liquid interface was easy to form a large ion concentration gradient, which was conducive to chemical reactions.

Author Contributions: Conceptualization, X.F.; methodology, X.F. and X.W.; software, X.W.; validation, X.F. and X.W.; formal analysis, X.W.; investigation, X.F. and X.W.; resources, X.F. and X.W.; data curation, X.W..; writing—original draft preparation, X.W.; writing—review and editing, X.F.; visualization, X.W.; supervision, X.F. and X.W.; project administration, X.F.; funding acquisition, X.F. All authors have read and agreed to the published version of the manuscript.

Funding: National Key R&D Program of China(2023YFC2907800) and Major Innovation Program of Shandong Province of China（2021CXGC011206）and Program of China University of Mining and Technology, grant number 2023WLKXJ015 and the Postgraduate Research & Practice Innovation Program of Jiangsu Province, grant number KYCX23_2774.

Data Availability Statement: Exclude this statement.

Acknowledgments: Thanks for the great effort by editors and reviewers.

Conflicts of Interest: The authors declare no conflict of interest.

References

1. Yang, X.; Xi, G.; Yao, N.; Zhou, M.; Gao, X.; Chen, M.; Wang, X.; Pan, Z.; Wang, Z. Spatiotemporal distribution of residual ammonium in a rare-earth mine after in-situ leaching: A modeling study with scarce data. J Hydrol 2022, 615.
2. Xiao, Y.; Feng, Z.; Hu, G.; Huang, L.; Huang, X.; Chen, Y.; Long, Z. Reduction leaching of rare earth from ion-adsorption type rare earths ore with ferrous sulfate. Journal of Rare Earths 2016, 34, (9), 917-923.
3. Huang, X.; Long, Z.; Wang, L.; Feng, Z. Technology development for rare earth cleaner hydrometallurgy in China. Rare Metals 2015, 34, (4), 215-222.
4. Artiushenko, O.; da Silva, R.; Zaitsev, V. Recent advances in functional materials for rare earth recovery: A review. Sustainable Materials and Technologies 2023, 37.

5. Wang, X.; Tang, Y.; Lee, J.; Fu, G. Recent advances in rare-earth-based materials for electrocatalysis. Chem Catalysis 2022, 2, (5), 967-1008.
6. Xiao, Y.; Feng, Z.; Huang X.; Huang, L.; Chen Y.; Wang, L.; Long, Z. Recovery of rare earths from weathered crust elution-deposited rare earth ore without ammonia-nitrogen pollution: I. leaching with magnesium sulfate. Hydrometallurgy 2015, 153, 58-65.
7. Traore, M.; Gong, A.; Wang, Y.; Qiu, L.; Bai, Y.; Zhao, W.; Liu, Y.; Chen, Y.; Liu, Y.; Wu, H.; Li, S.; You, Y. Research progress of rare earth separation methods and technologies. Journal of Rare Earths 2023, 41, (2), 182-189.
8. Jing, H.; Geng, L.; Qiu, S.; Zou, H.; Liang, M.; Deng, D. Research progress of rare earth composite shielding materials. Journal of Rare Earths 2023, 41, (1), 32-41.
9. He, Q.; Qiu, J.; Chen, J.; Zan, M.; Xiao, Y. Progress in green and efficient enrichment of rare earth from leaching liquor of ion adsorption type rare earth ores. Journal of Rare Earths 2022, 40, (3), 353-364.
10. Shen, L.; Zhou, H.; Shi, Q.; Meng, X.; Zhao, Y.; Qiu, G.; Zhang, X.; Yu, H.; He, X.; He, H.; Zhao, H. Comparative chemical and non-contact bioleaching of ion-adsorption type rare earth ore using ammonium sulfate and metabolites of Aspergillus niger and Yarrowia lipolytica to rationalise the role of organic acids for sustainable processing. Hydrometallurgy 2023, 216, 106019.
11. Lai, F.; Huang, L.; Gao, G.; Yang, R.; Xiao, Y. Recovery of rare earths from ion-absorbed rare earths ore with $MgSO_4$ -ascorbic acid compound leaching agent. Journal of Rare Earths 2018, 36, (5), 521-527.
12. Deng, Y.; Wan, Y.; Yu, H.; Kang, S.; Deng, Y.; Yang, J. Changes in Microfine Particle Migration of Ionic Rare Earth Ores during Leaching. Sustainability 2023, 15, (4).
13. Lai, F.; Gao, G.; Huang, L.; Xiao, Y.; Yang, R.; Li, K. Compound leaching of rare earth from the ion-adsorption type rare earth ore with magnesium sulfate and ascorbic acid. Hydrometallurgy 2018, 179, 25-35.
14. Ran, X.; Ren, Z.; Gao, H.; Zheng, R.; Jin, J. Kinetics of Rare Earth and Aluminum Leaching from Kaolin. Minerals 2017, 7, (9).
15. Chi, R.; Tian, J.; Li, Z.; Peng, C.; Wu, Y.; Li, S.; Wang, C.; Zhou, Z. Existing State and Partitioning of Rare Earth on Weathered Ores. Journal of Rare earth 2005, (06), 756-9+643.
16. Chen, J.; Qiu, J.; Huang, L.; Chen, X.; Yang, Y.; Xiao, Y. Coordination–reduction leaching process of ion-adsorption type rare earth ore with ascorbic acid. Journal of Rare Earths 2023, 41, (8), 1225-1233.
17. Xiao, Y.; Feng, Z.; Hu, G.; Huang, L.; Huang, X.; Chen, Y.; Li, M. Leaching and mass transfer characteristics of elements from ion-adsorption type rare earth ore. Rare Metals 2015, 34, (5), 357-365.
18. Meng, X.; Zhao, H.; Zhao, Y.; Shen, L.; Gu, G.; Qiu, G. Heap leaching of ion adsorption rare earth ores and REEs recovery from leachate with lixiviant regeneration. Science of The Total Environment 2023, 898, 165417.
19. Guo, Z.; Zhou, J.; Zhou, K.; Jin, J.; Wang, X.; Zhao, K. Soil-water characteristics of weathered crust elution-deposited rare earth ores. Transactions of Nonferrous Metals Society of China 2021, 31, (5), 1452-1464.
20. Wang, L.; Wang, C.; Li, L.; Yang, Y. Readsorption of rare earth elements during leaching process of ion-adsorption-type rare earth ore. Rare Metals 2018, 42, (6), 2113-2120.
21. Xiao, Y.; Gao, G.; Huang, L.; Feng, Z.; Lai, F.; Long, Z. A discussion on the leaching process of the ion-adsorption type rare earth ore with the electrical double layer model. Minerals Engineering 2018, 120, 35-43.
22. Yu, H.; Sun, D. Effect of NaCl solution on swelling of bentonite with different water contents. In NEW ADVANCES IN GEOTECHNICAL ENGINEERING 2018, 455-459.
23. Alkan, M.; Karadaş, M.; Doğan, M.; Demirbaş, Ö. Zeta potentials of perlite samples in various electrolyte and surfactant media. Colloids and Surfaces A: Physicochemical and Engineering Aspects 2005, 259, (1-3), 155-166.
24. Wu, Z.; Chen, Y.; Wang, Y.; Xu, Y.; Lin, Z.; Liang, X.; Cheng, H. Review of rare earth element (REE) adsorption on and desorption from clay minerals: Application to formation and mining of ion-adsorption REE deposits. Ore Geology Reviews 2023, 157.
25. Wang, L.; Liao, C.; Yang, Y.; Xu, H.; Xiao, Y.; Yan, C. Effects of organic acids on the leaching process of ion-adsorption type rare earth ore. Journal of Rare Earths 2017, 35, (12), 1233-1238.
26. Xiao, Y.; Chen, Y.; Feng, Z.; Huang, X.; Huang, L.; Long, Z.; Cui, D. Leaching characteristics of ion-adsorption type rare earths ore with magnesium sulfate. T Nonferr Metal Soc 2015, 25, (11), 3784-3790.
27. Feng, J.; Zhou, F.; Chi, R.; Liu, X.; Xu, Y.; Liu, Q. Effect of a novel compound on leaching process of weathered crust elution-deposited rare earth ore. Minerals Engineering 2018, 129, 63-70.
28. Hu, G.; Feng, Z.; Dong, J.; Meng, X.; Xiao, Y.; Liu, X. Mineral properties and leaching characteristics of volcanic weathered crust elution-deposited rare earth ore. Journal of Rare Earths 2017, 35, (9), 906-910.
29. Yin, S.; Pei, J.; Jiang, F.; Li, S.; Peng, J.; Zhang, L.; Ju, S.; Srinivasakannan, C. Ultrasound-assisted leaching of rare earths from the weathered crust elution-deposited ore using magnesium sulfate without ammonia-nitrogen pollution. Ultrason Sonochem 2018, 41, 156-162.

30. Shi, Q.; Zhao, Y.; Meng, X.; Shen, L.; Qiu, G.; Zhang, X.; Yu, H.; He, X.; He, H.; Zhao, H. Column leaching of ion adsorption rare earth ore at low ammonium concentration. Journal of Materials Research and Technology 2022, 19, 2135-2145.
31. Rasoulnia, P.; Barthen, R.; Lakaniemi, A. A critical review of bioleaching of rare earth elements: The mechanisms and effect of process parameters. Critical Reviews in Environmental Science and Technology 2020, 51, (4), 378-427.
32. Xie, F.; Yin, S.; Yuan, C.; Qi, Y.; Liang, J.; Zhu, Z.; Li, G. Study on the Influence Mechanism of Leaching Solution on Pore of Ionic R are Earth Ore. Chinese Rare Earths, 2018, 39(06): 48-56.
33. Zhang, J.; Zheng, F.; Liu, Z.; Hong, S.; Dong, B.; Xing, F. Nondestructive monitoring on hydration behavior of cement pastes via the electrochemical impedance spectroscopy method. Measurement 2021, 185.
34. Liu, Q.; Cheng, S.; Xiao, J.; Sun, C. Study of the relationship between the AC impedance spectrum of varied building solid waste materials and their microporous structure[J]. Journal of Building Materials: 1-11.
35. Bragança, M.; Hasparyk, N.; Bronholo, J.; Silva, A.; Portella, K.; Kuperman, S., Electrochemical impedance spectroscopy and ultrasound for monitoring expansive reactions and their interactions on cement composites. Construction and Building Materials 2021, 305.
36. Rao, R.; Sasmal, S. Nanoengineered smart cement composite for electrical impedance-based monitoring of corrosion progression in structures. Cement and Concrete Composites 2022, 126.
37. Wen, W.; Jia, L.; Xie, J.; Zhao, W.; Feng, H.; Cao, D.; Sun, F.; Han, P.; Bai, X.; He, B. Electrochemical response and effect evaluation of high belite sulphoaluminate cement combined with red mud-fly ash on solidification of Cu^{2+}-contaminated kaolin. Case Studies in Construction Materials 2022, 17.
38. Barsoukov. Impedance Spectroscopy: Theory, Experiment, and Applications, 3rd ed.; Wiley-Interscience; Hoboken, USA, 2005.
39. Shi. Impedance Spectroscopy of Concrete; China Railway Publishing House: Beijing, China, 2003.
40. Cao.; Zhang. Introduction to Electrochemical impedance spectroscopy.; Science Press: Beijing, China, 2002.
41. Zhao, S.; Guo, B.; Peng, Y.; Mai, Y. An impedance spectroscopy study on the mitigation of clay slime coatings on chalcocite by electrolytes. Minerals Engineering 2017, 101, 40-46.
42. Elmelouky, A.; Mortadi, A.; Chahid, E.; Elmoznine, R. Impedance spectroscopy as a tool to monitor the adsorption and removal of nitrate ions from aqueous solution using zinc aluminum chloride anionic clay. Heliyon 2018, 4, (2), e00536.
43. Han, P.; Zhang, Y.; Chen, F.; Bai, X. Interpretation of electrochemical impedance spectroscopy (EIS) circuit model for soils. Journal of Central South University 2015, 22, (11), 4318-4328.
44. Sun, F.; Chen, Z.; Bai, X.; Wang, Y.; Liu, X.; He, B.; Han, P. Theoretical and experimental bases for the equivalent circuit model for interpretation of silty soil at different temperatures. Heliyon 2023, 9, (2), e12652.
45. Cheng, J. Experimental study on the electrochemical characterization of kaolin and montmorillonite. Taiyuan University of Technology, Taiyuan, Shanxi, China, 2022.
46. Niu, S.; Luo, J.; Chen, M.; Chen, Z.; Wang, X.; Bai, X.; Li, J. Experimental study of cement-based materials under sulfate attack environment using Electrochemical Impedance Spectroscopy. International Journal of Electrochemical Science 2023, 18, (5).
47. Niu, S.; Wang, X.; Xing, J.; Li, J.; Xie, R.; Bai, X.; Han, P. Experimental Study of the Electrochemical Impedance Characteristics and Mechanical Properties of High Belite Sulfoaluminate Cement. International Journal of Electrochemical Science 2022, 17, (12).
48. Wang, H.; Wang, X.; Wang, Y.; Wang, D.; Hu, K.; Zhong, W.; Guo, Z. Influence of ammonium sulfate leaching agent on engineering properties of weathered crust elution-deposited rare earth ore. Acta Geotechnica 2023.
49. Wang, X.; Zhuo, Y.; Zhao, K.; Zhong, W. Experimental measurements of the permeability characteristics of rare earth ore under the hydro-chemical coupling effect. RSC Adv 2018, 8, (21), 11652-11660.
50. Gao, Z.; Rao, Y.; Shi, L.; Xiang, R.; Yang, Z. Effect of Magnesium Sulfate Solution on Pore Structure of Ionic Rare Earth Ore during Leaching Process. Minerals 2023, 13, (2).
51. Zhou, L.; Wang, X.; Huang, C.; Wang, H.; Ye, H.; Hu, K.; Zhong, W. Development of pore structure characteristics of a weathered crust elution-deposited rare earth ore during leaching with different valence cations. Hydrometallurgy 2021, 201.
52. Zhang, X.; Gao, Z.; Rao, Y.; Shi, L.; Xu, W. Evolutionary Law of Pore Structure of Ion-Adsorbed Rare Earth Ore Leaching Process. Minerals 2023, 13, 322.
53. Shi, L.; Rao, Y.; Wang, D.; Zhang, M.; Huang, T.; Gao, Y. A Capillary Model for Predicting Saturated Hydraulic Conductivity of Ion-Adsorption Rare Earth Ore Based on Improved Kozeny–Carman Equation. Geofluids 2022, 2022, 1-10.
54. Luo, X.; Zhang, Y.; Zhou, H.; He, K.; Zhang, B.; Zhang, D.; Xiao, W. Pore structure characterization and seepage analysis of ionic rare earth orebodies based on computed tomography images. International Journal of Mining Science and Technology 2022, 32, (2), 411-421.

55. Xie, R.; Xie, Y.; Li, B.; Han, P.; He, B.; Dou, B.; Bai, X. Electrochemical Impedance Spectroscopy of Sandy Soil Containing Cl-, SO42- and HCO3. International Journal of Electrochemical Science 2021, 16, (12).
56. Long, P.; Wang, G.; Zhang, C.; Yang, Y.; Cao, X.; Shi, Z. Kinetics model for leaching of ion-adsorption type rare earth ores. Journal of Rare Earths 2020, 38, (12), 1354-1360.
57. Wang, X.; Zhuo, Y.; Deng, S.; Li, Y.; Zhong, W.; Zhao, K. Experimental Research on the Impact of Ion Exchange and Infiltration on the Microstructure of Rare Earth Orebody. Advances in Materials Science and Engineering 2017, 1-8.